SAND2000-1960 C

Design of the PST: A Diagnostic for 1-D Imaging of Fast Z-pinch Power Emissions

G.A. Rochau, M.S. Derzon, G.A. Chandler
Sandia National Laboratories, Albuquerque, NM 87185
S.E. Lazier
Ktech Corp., Albuquerque, NM

Fast Z-pinch technology developed on the Z machine at Sandia National Laboratories can produce up to 230 TW of thermal x-ray power for applications in inertial confinement fusion (ICF) and weapons physics experiments. During implosion, these Z-pinches develop Rayleigh-Taylor (R-T) instabilities which are very difficult to diagnose and which functionally diminish the overall pinch quality. The Power-Space-Time (PST) instrument is a newly configured diagnostic for measuring the pinch power as a function of both space and time in a Z-pinch. Placing the diagnostic at 90 degrees from the Z-pinch axis, the PST provides a new capability in collecting experimental data on R-T characteristics for making meaningful comparisons to magneto-hydrodynamic computer models. This paper is a summary of the PST diagnostic design. By slit-imaging the Z-pinch x-ray emissions onto a linear scintillator/fiber-optic array coupled to a streak camera system, the PST can achieve ~100 μm spatial resolution and ~1.3 ns time resolution. Calculations indicate that a 20 μm thick scintillating detection element filtered by 1000 Å of Al is theoretically linear in response to Plankian x-ray distributions corresponding to plasma temperatures from 40 eV to 150 eV. By calibrating this detection element to x-ray energies up to 5000 eV, the PST can provide pinch power as a function of height and time in a Z-pinch for temperatures ranging from ~40 eV to ~400 eV. With these system parameters, the PST can provide data for an experimental determination of the R-T mode number, amplitude, and growth rate during the late-time pinch implosion.

1. Introduction

The Z machine at Sandia National Laboratories is a driver of fast z-pinches to produce high-intensity x-ray environments for applications in Inertial Confinement Fusion (ICF) and weapons physics experiments [1]. The basic theory of z-pinches applies to this configuration where the current carrying load is typically a 1 cm tall, 4 cm diameter cylindrical wire array composed of > 300 Tungsten wires with diameters of ~7.5 μm [2]. These z-pinches are driven by a 100 ns current pulse peaked at 20 MA which delivers a total energy of ~2 MJ to the z-pinch load. As the wires vaporize under the high energy density of the current pre-pulse, they form a fairly uniform plasma sheath which conducts the bulk of the main current pulse and radially implodes under its own magnetic field. The plasma sheath typically collides onto a low-density plastic foam located central to the z-pinch with a radius of ~2.5 mm and a density of ~7 mg/cc. As the pinch compresses this foam, the sheath becomes opaque to its own emission and internally reaches temperatures as high as 230 eV (2.7 million degrees centigrade). Before the pinch disassembles, it can radiate 1.9 MJ of x-ray energy in a 5 – 10 ns wide pulse corresponding to peak powers up to 230 TW.

The dynamics of the z-pinch implosion, such as sheath thickness and radiation pulse width, are dictated in large part by the magnitude and growth rate of Rayleigh-Taylor (R-T) instabilities [3]. These instabilities are a hydrodynamic phenomenon instigated by the perturbation of a boundary where a higher-density fluid is supported by a lower-density fluid [4]. In the case of a z-pinch, the magnetic field acts as a zero density fluid which drives the finite density plasma such that perturbations in the tungsten plasma or in the magnetic field can seed an R-T instability. The theory behind the wavelength and growth rates of these instabilities is not well understood, and computer modelers must adjust these parameters (without any physical justification) until the simulations match the experimental pulse widths and radiation levels [5]. This impedes the understanding of the basic z-pinch physics and makes it difficult to predict the performance of future experiments that utilize untried load parameters. Fig. 1 shows the density contours of a 2-D computer simulation demonstrating the wavelength and magnitude of the theoretical R-T

DISCLAIMER

instabilities. This simulation was conducted with a radiation-hydrodynamics code called ALEGRA [6]. The long plasma 'fingers' which extend away from the front of the sheath are referred to as spikes while the curved surfaces of the voids between spikes are referred to as bubbles.

Diagnosing the actual wavelength and growth rates of R-T bubbles and spikes in z-pinch experiments is central to understanding the z-pinch physics. However, these measurements are difficult to accomplish in the harsh environment created by the Z machine. Protection from Electro-Magnetic-Pulse (EMP) generated in the machine diode requires that any electrical diagnostics be placed in faraday cages. Additionally, the high levels of radiation produced by a z-pinch often require that sensitive diagnostics be placed far from the machine center. Due to the Z machine geometry, most diagnostics which view the z-pinch from the side must do so at a 78° angle from the pinch axis. This variance from a 90° viewing angle complicates the experimental measurements, especially when comparing to computer models which inherently view the pinch process from 90°. Thus, there is a need in the diagnostic suite on the Z machine for an instrument which can image the z-pinch emissions at 90° for the purpose of measuring the R-T characteristics, and for comparing the measured overall pinch emissions at 90° to those at 78°.

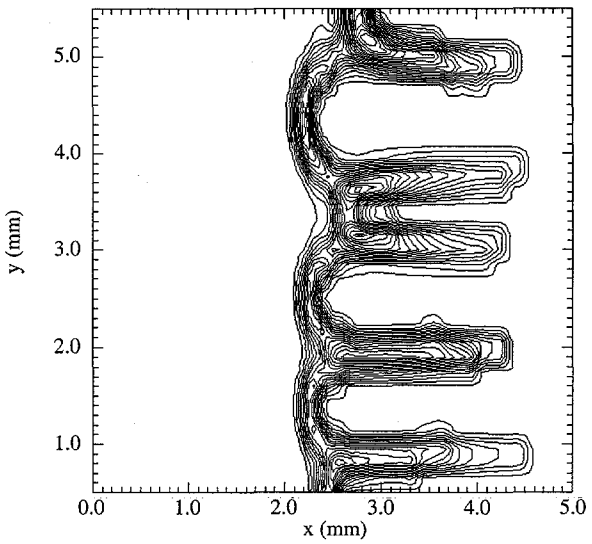

Fig. 1: Density contours from an ALEGRA simulation of a z-pinch on Sandia's Z-machine. R-T structure shows a wavelength of ~ 1mm.

This paper describes the design of the Power-Space-Time (PST) diagnostic for making 1-D images of z-pinch power emissions at 90° from the pinch axis on the Z machine. This is a fiber-optic based diagnostic with variable magnification which relies on scintillator detection to provide power resolution, slit imaging to provide spatial resolution, and a streak camera to provide time resolution.

2. Design Parameters

The PST is an adaptation of a one-dimensional imaging system developed originally for measuring target x-ray emissions on PBFA II. However, since the conversion of PBFA II to the present day Z machine, work has been done to adapt the instrument for use in measuring relative intensity as a function of height or radius in a z-pinch. The diagnostic consists of a slit aperture which projects a one-dimensional image of the pinch radiated x-rays onto a thin aluminum filtered, scintillator coated fiber-optic faceplate. This faceplate is coupled directly to three linear fiber-optic arrays that extend from the machine center to an externally located faraday cage or screen box. The light from the fiber arrays is focused onto a streak camera photocathode and the resulting space- and time-resolved image is captured on a computer controlled CCD. Schematics of the PST are shown in figs. 1(a), 1(b), and 1(c). The three linear arrays shown in fig. 1(b) are each composed of 120 fibers stacked one on top of the other. These fibers are radiation hardened fused silica with a 100 μm core diameter and a 127 μm outer diameter. The two outer arrays are for radiation detection while the center array contains 2 fibers for alignment and four sets of 3 fibers for making coupling and focusing measurements at shot time. The scintillator is spin coated on the source side of the fiber-optic faceplate mounted to the flange shown here. The spin coating procedure can deposit scintillator layers from 1 μm to 20 μm thick with about a 1% uniformity. Fig. 1(c) shows the alignment of the PST within the Z machine target chamber as placed to achieve maximum magnification and spatial resolution.

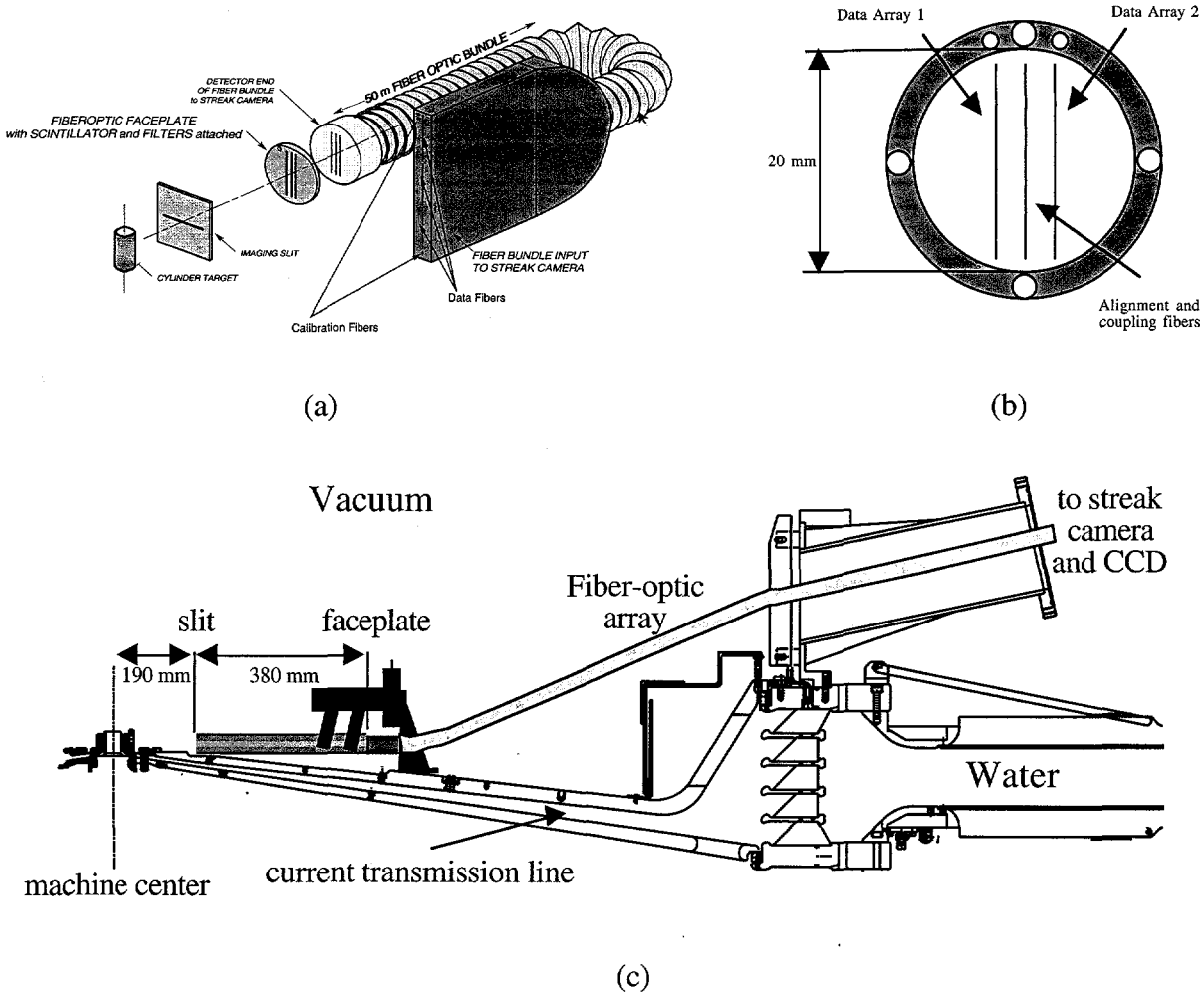

Fig. 2: (a) Schematic of the PST fiber-optic imaging assembly. (b) Detail of the PST fiber-optic faceplate and mounting flange. The 3 linear fiber-optic arrays are butte coupled to the back face. (c) Schematic of the PST hardware assembly as fielded on the Z machine. This configuration yields a x2 magnification.

2.1 Scintillator and Filter design

The active element of the PST is a fast scintillator developed at Bicron called BC-422Q. This is a polyvinyltoluene based plastic organic scintillator which contains 0.5% Benzophenone for quenching of longer time-scale light emissions. The listed timing characteristics of the light output for BC422Q are a 110 ps rise time, a 360 ps full-width-at-half-max (FWHM), and a 700 ps decay time [7]. The response of this scintillator to soft x-ray spectra from 10 nm up to 3000 nm has not been measured in detail, but the percentage of light output is believed to scale linearly with the amount of energy deposited. Thus, we have modeled the detector response by calculating the absorption fraction as a function of x-ray energy for polystyrene plastic which has an atomic composition and density similar to that of the BC-422Q scintillator. These calculations were conducted with the XRD radiation detector design code which references the Biggs and Lighthill x-ray cross section approximations to plot transmission or absorption fractions as a function of x-ray energy [8,9]. The results of these calculations for a number of polystyrene thicknesses are shown in fig. 3 for x-ray energies up to 10 KeV. The dip in x-ray absorption which occurs between 100 and 300 eV corresponds to the 284.2 eV K shell binding energy of the carbon in plastic. Fig. 3 indicates that the scintillator must be at least 20 μm thick to overcome the absorption reduction in

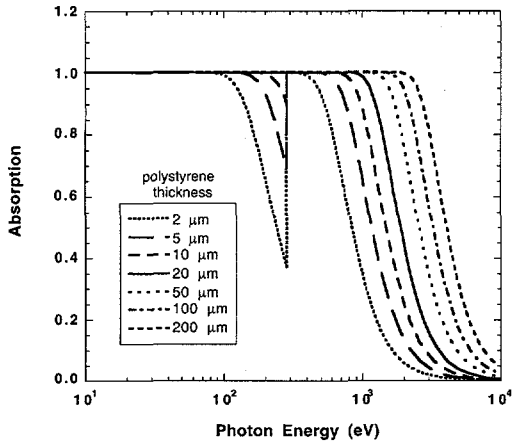

Fig. 3: XRD calculated polystyrene x-ray absorption fractions for various thicknesses. The absorption dip corresponds to the Carbon K shell.

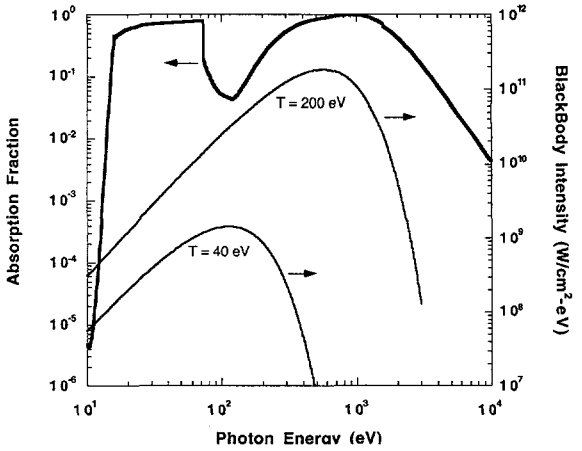

Fig. 4: Absorption fraction for 20 μm polystyrene filtered by 1000 Å of Al. Also shown are Plankian spectra for a 40 eV and 200 eV plasma.

this energy range. At this thickness, the scintillator absorption fraction is flat up to 850 eV, and falls down to 40% for x-ray energies of 2000 eV. If the scintillator response must be flat up to 2000 eV, then a 200 μm scintillator layer is required.

Many x-ray diagnostics on the Z machine rely on multiple filters to measure the magnitude of the differential spectral emissions which are theoretically compared to determine the emitted x-ray power [10]. This method provides some insight into the spectrum emitted by the target, but relies on the theoretical understanding of the detector response to determine the absolute power. The PST diagnostic takes a different approach. The z-pinch radiation produced on the Z machine has been measured to have a dominantly Plankian spectrum. This blackbody signature has a different total x-ray energy output for every temperature (power) produced by the z-pinch. Therefore, if the PST response is measured for a range of energies absorbed in the scintillator, then it can be calibrated to measure z-pinch radiated power without resolving the details of the pinch spectrum. The best way to measure the total blackbody power is to have a detector with a linear response for x-ray energies up to 3000 eV. However, the x-ray radiation between the source and the scintillator must be filtered to prevent unwanted visible light from entering the fiber-optic array. The thermal x-rays which the PST are intended to measure are not very penetrating such that only a very thin filter can be used. The best candidate for achieving this optical filtering is Aluminum, which can be sputter coated in layers as thin as a few hundred Angstroms. To achieve reliable light-blocking with an Al sputter coat, the required filter thickness has been determined to be ~1000 Å. The absorption fraction of a 20 μm polystyrene based scintillator with a 1000 Å Al filter is shown in fig. 4 along with the Plankian spectra of both a 40 eV and a 200 eV plasma. As can be seen in the figure, the Al L shell edge at 72.9 eV reduces the scintillator absorption to as low as 5% between 73 eV and about 400 eV. This significantly removes the linearity of the scintillator response and thus makes calibration a more difficult issue. However by calibrating to a known x-ray energy spectra, the effect of this shell edge can be accounted for.

In order to develop a simulated PST response to a given blackbody emission spectrum, we folded Plankian spectral distributions for plasma temperatures from 40 eV up to 400 eV into the scintillator response shown in fig. 4. This is done by integrating the product of the differential scintillator absorption fraction, A_E, and the differential blackbody power, dP/dE, in the equation:

$$\text{Res.} = \int_0^\infty A_E \frac{dP}{dE} dE. \qquad (1)$$

The differential blackbody power is given (averaged over steradians) by the equation:

$$\frac{dP}{dE} = (1.26 * 10^3)\frac{E^3}{e^{\frac{E}{T}} - 1} \quad \left\{\frac{\mathrm{W}}{\mathrm{cm^2 eV}}\right\} \quad (2)$$

for T the blackbody temperature. The result of this calculation for a wide range of powers is shown in fig. 5. According to this figure, the response of the scintillator is theoretically linear for z-pinch powers up to about 100 TW. For powers over 100 TW, the PST scintillator response becomes non-linear due to the drop in absorption of the scintillator layer. This effect can be reduced by using a thicker scintillator, but the trade-off is a decline in spatial resolution as discussed in the next section.

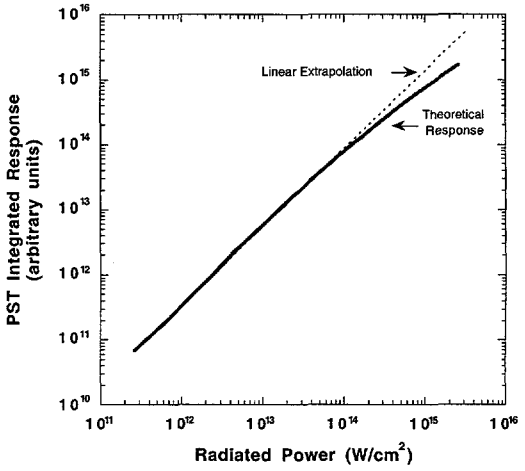

Fig. 5: Theoretical scintillator response to Plankian spectra up to a blackbody temperature of 400 eV.

2.2 Spatial and Temporal Resolution

There are 3 components which contribute to the spatial resolution of the PST. These are the fiber-optic size, geometric spot size, and x-ray diffraction. The fiber limited resolution is determined by the size and separation of the fiber-optics in the detector array. The PST array is composed of 120 fibers with a center-to-center separation of 127 μm. Thus, the fiber limited minimum spot size on the detector face, d_f, is 127 μm. The second component, the geometric spot size, is defined as the image size of a point source which the slit imposes on the detector face. This is a function of the detector placement geometry and can be determined from the equation:

$$d_s = w(M+1) \quad (3)$$

where w is the width of the slit and M is the PST magnification. The third component which contributes to the resolution limit is due to x-ray diffraction . This is calculated by the Fresnel diffraction approximation which assumes that the x-rays approach the slit as plane waves with normal incidence [11]. The diffraction induced spot size then corresponds to the width of the first minimum in the diffraction pattern and can be calculated by:

$$d_d = \frac{hc}{Ew} L \quad (4)$$

where h is Planck's constant, c is the speed of light, E is the energy of the x-ray, and L is the distance between the slit and the detector face. These 3 components can be added in quadrature to determine a conservative estimate of the overall detector resolution at the source, R_s, by the equation:

$$R_s = \sqrt{d_f^2 + d_s^2 + d_d^2}\,/M. \quad (5)$$

This is not the only way to determine an estimate of the spatial resolution. The least conservative method is to compare each of the resolution components, select the one which dictates the maximum detector spot size, and set the theoretical spatial resolution to that value. If the three components in eq. 5 are approximately the same, then this less conservative method will lead to a spatial resolution which is a factor of 1.7 less than that indicated by eq. 5. The true spatial resolution is likely somewhere in between and requires a detailed measurement of the edge spread function of this system to determine the true PST spatial resolution.

The spatial resolution given in eq. 5 is a function of the x-ray energy, and the PST is designed to look at a Plankian distribution of energies. Therefore, the resolution of the PST will also be a function of the z-pinch temperature. To calculate the conservative spatial resolution of the PST diagnostic, we again must fold the Plankian spectral distribution into the PST spatial response in order to determine the resolution as a function of z-pinch power. This is done by solving the equation:

$$\langle R_s \rangle = \frac{\int R_s \frac{dP}{dE} dE}{\int \frac{dP}{dE} dE}. \qquad (6)$$

The results of these calculations are shown in fig. 6 for magnification levels of 2 and 0.65, corresponding to source to slit distances of 195 mm and 597 mm respectively. If the slit is placed at 190 mm from the target and the scintillator detection element is placed at 390 mm from the slit, then the magnification is a factor of 2 and the PST can achieve between 100 μm and 110 μm resolution at the source.

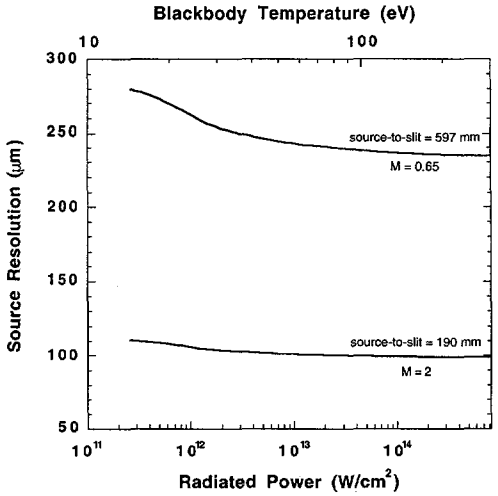

Fig. 6: Spectrally averaged spatial resolution of the PST at select source-to-slit distances and magnifications.

There is one other component of the spatial resolution which was not considered in the analysis above, the fiber cross-talk. The fiber cross-talk is determined by the separation between the fiber-optic array and the scintillator. In the PST, the scintillator is coated directly onto a fiber-optic faceplate composed of many small fibers that have been extruded and compressed. In the PST system, this faceplate is made of 11 μm diameter fibers which have a numerical aperture of 0.66. The fiber-optic array is butte coupled to the back of the faceplate such that there is no cross-talk between the faceplate and the array. However, if light is produced in an area of the scintillator which is within the numerical aperture of two fibers in the faceplate, and these fibers have a direct line of sight to two different fibers in the array, then some cross-talk can occur between channels. The thicker the scintillator layer on the PST detection element, the larger the fiber-to-fiber cross-talk. Geometric analysis indicates that this is a very small effect for scintillator thicknesses less than about 50 μm. A true measurement of the fiber cross-talk can be measured by determining the edge spread function of the PST system without a slit aperature by simply masking a portion of the scintillator.

The temporal resolution of the PST can be estimated by an analysis of the scintillator response time, the CCD pixel induced time resolution, and the intermodal temporal broadening in the fiber-optics. As was mentioned above, the scintillator response time has a FWHM of only 360 ps which is a general figure of merit for the time resolution. However, with a continuous radiation source incident on the scintillator, the light decay time can add significantly to the later time signal. A radiation source which emits as a delta function in time would induce a scintillator light output for a total time of about 1.2 ns. Additionally, because the light from the fiber array is streaked across the face of a CCD camera, the individual pixels in the CCD induce another limitation on the time resolution. Typically, the streak camera is set to a 50 ns sweep time such that each pixel on a 1024 x 1024 CCD chip represents approximately 50 ps. The third component of the PST time resolution, the intermodal temporal broadening of the fiber-optics, depends on the length of fiber and the numerical aperture. The details of this calculation are not included here, but can be shown to yield an intermodal broadening of 500 ps for a 25 ft. length of the PST fiber [12]. These three values can be added in quadrature to yield a total system time resolution of ~ 1.3 ns. The actual time resolution of the PST diagnostic should be within ± 0.1 ns of this value. The only way to determine the actual time resolution of the PST system is to measure it with a sharp radiation pulse that emits for only ~10 ps.

3. Experimental Data

A predecessor to the PST diagnostic has been fielded on the Z machine for a number of shots to gain some insight into the theory as described above. The diagnostic consists of two fiber-optic arrays containing 60 fibers each and arranged in the same configuration as described in

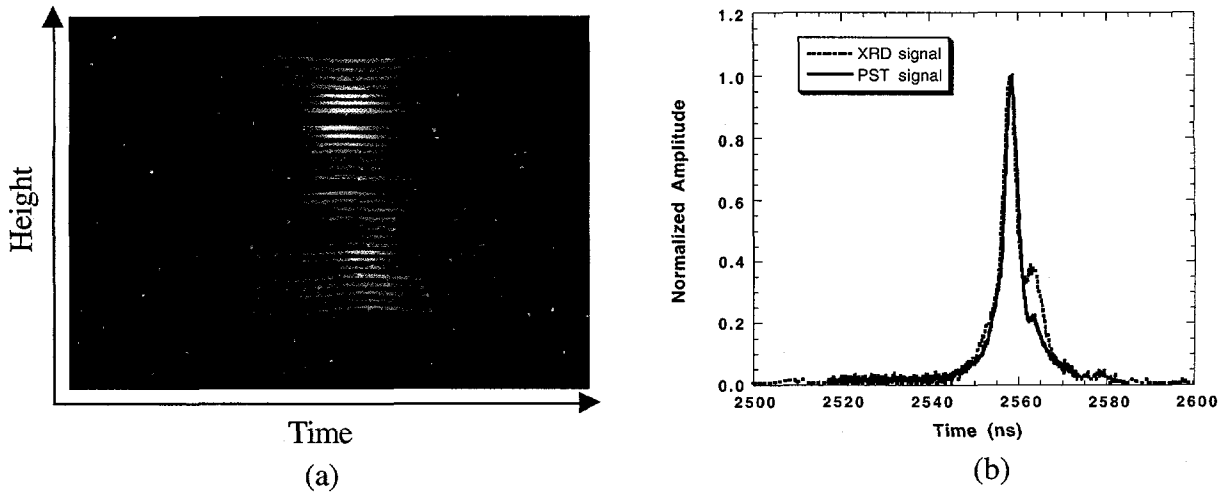

Fig. 7: (a) PST streak image from Z shot 600. The pinch field of view is about 5 mm and the window width represents about 40ns. (b) Comparison of the XRD signal to the spatially integrated PST amplitude.

section 2. This uncalibrated PST has been fielded at source-to-slit distances of 190 mm and 597 mm with magnifications ranging from 0.35 to 2.

Fig. 7(a) shows a post-processed PST image from Z shot 600 where the x axis is time and the y axis corresponds to the distance in height along the z-pinch. This was a 1 cm tall,40 cm diameter tungsten wire array on a 5 mm diameter, 7.5 mg/cc TPX foam. The PST was located at a source-to-slit distance of 597 mm with a magnification of 0.65. In this case, the PST was filtered with a 2.13 μm thick aluminized kimfol filter for the purpose of comparing the PST measured power profile to that of the Z machine's X-ray Diodes (XRDs). Fig. 7(b) shows this comparison by taking a spatially summed lineout over the height of the z-pinch and plotting the result against the XRD measured response. These power profiles overlay quite well indicating that the PST is measuring power emissions with the appropriate linearity. The one exception to this is the magnitude of the second rise which occurs ~ 3 ns after the main peak. The PST shows a lower second peak than the XRD which raises some questions as to the late time response of the PST. The XRD looks at the z-pinch at a78° angle from the pinch axis such that it also looks at the cathode of the Z machine diode. If this second bump were a machine cathode effect than it would be quite a bit brighter in the XRD signal than the PST. The other possible explanation is that the high x-ray flux of the main peak may partially saturate the PST scintillator such that later time signals are washed out by the long decay time of the scintillator light output. More detailed investigation of this late time response needs to be conducted for a variety of power profiles to determine its true effect.

The uncalibrated PST has also been fielded on a few shots to look specifically at the R-T structure of the z-pinch as it evolves in time. Fig. 8 shows a post-processed PST image of Z shot 616. This z-pinch configuration was a 20 mm tall, 40 mm diameter tungsten wire array on a 10 mm diameter, 5 mg/cc foam. The 100 μm PST imaging slit was located 724 mm from the z-pinch axis while the fiber-optic faceplate was located 163 mm from the slit. This gave a source magnification of 0.36 and a field of view at the target of 21 mm. The PST image is corrupted by both broken fibers, and a cracked spectral band-pass filter at the streak camera. Thus, the actual field-of-view for useful PST data is about 12 mm. However, the early time PST image shows a definite pinch structure as the tungsten sheath strikes the center foam which looks very much like the R-T instability shown in fig. 1. The main difference is that this PST image indicates an R-T wavelength of about 2 mm while computer simulations tend to indicate a dominant 1 mm wavelength at this time in the pinch implosion. Additionally, the data in fig. 8 indicates that the R-T wavelength which is present when the tungsten sheath strikes the foam is the same wavelength and structure which exists when the pinch stagnates on-axis. However, because of the high de-

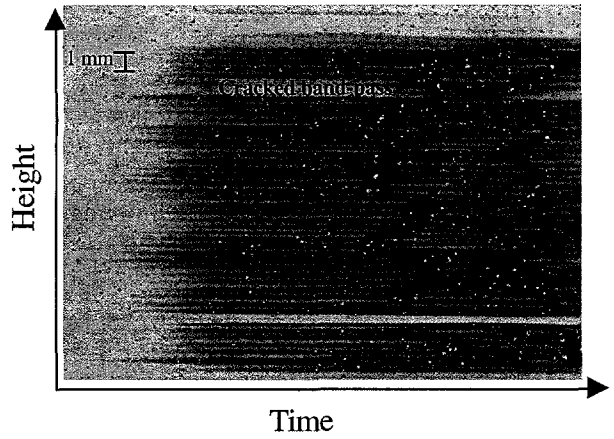

Fig. 8: PST streak of Z shot 616. The total field of view is 20 mm and the window width represents about 28 ns. Spatial resolution is estimated at 400 μm.

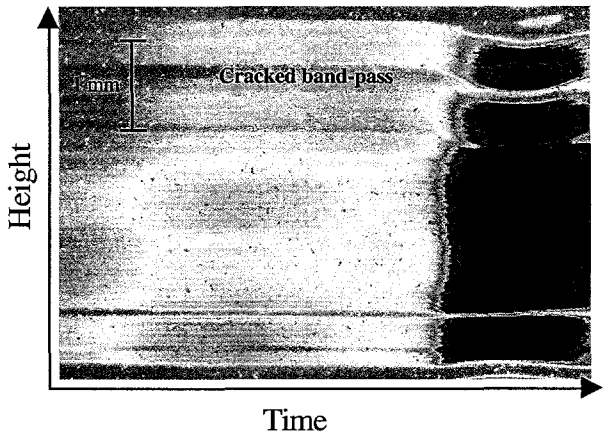

Fig. 9: PST streak of Z shot 615. The total field of view is 3.8 mm and the window width represents about 16 ns. Spatial resolution is estimated at 100 mm.

magnification , the large source-to-slit distance in this setup, and the fairly large 100 μm slit aperture, the source resolution of the PST on this shot was only ~400 μm. This can lead to an aliasing effect which makes the wavelength of repetitive small features, such as an R-T instability, seem longer than it is [13]. Calculations have been done which indicate that the PST would need at least 120 μm resolution at the source to measure a 1 mm R-T wavelength with no aliasing. The data in fig. 8 is not a loss, however, because it indicates that the PST can in fact image features with varying degrees of brightness along the length of the z-pinch.

To obtain data with a high degree of spatial resolution and eliminate the effect of aliasing, the uncalibrated predecessor to the PST was also fielded in the configuration shown in fig. 2. This provides a x2 magnification and a spatial resolution between 100 μm and 110 μm at the source. The data from this configuration as fielded on Z shot 614 is shown in fig. 9. The load on this shot was a 15 mm tall, 40 mm diameter tungsten wire array with a 20 mm diameter tungsten nested wire array on a 10 mm diameter, 50 mg/cc foam. The drawback of the PST configuration with this smaller fiber-optic array is that it only provides a 3.8 mm field of view at the target. With the broken fibers and cracked band-pass filter, this only allows for about 2.5 mm of useful data. As can be seen from fig. 9, there is a spatial structure which is evident over this 2.5 mm. If we assume that this is due to an R-T instability, it would correspond to a wavelength of about 1.5 mm. The problem with this data is that there is not a large enough field of view to conclusively say whether the structure is due to an R-T instability or some other anomaly which induces an asymmetry in the z-pinch.

4. Discussion

The theoretical design of the PST indicates that this diagnostic could provide a new capability for measuring z-pinch power emissions at 90° from the z-pinch axis with ~100 μm spatial resolution and ~1.3 ns time resolution. In addition, preliminary experimental data indicates that the PST imaging system behaves in a manner similar to that dictated by theory. The next step in the development of this diagnostic is to increase the overall field of view of the PST and calibrate the scintillator detection element. This diagnostic could then provide 1-D images of the R-T emission amplitudes and wavelengths with high spatial fidelity for conducting detailed comparisons to computer models. It should be noted, however, that these comparisons will require a detailed understanding of the z-pinch plasma opacities in order calculate the theoretical spectra at the PST location. This is a difficult problem which requires very accurate computer modeling in order to generate data that can be compared in a meaningful manner. There is a large ongoing effort at Sandia National Laboratories to develop this kind of detailed modeling. If these efforts are successful, and the PST can be demonstrated to make the kind of measurements

described in this paper, then we will have come a long way in understanding the finer details of fast z-pinch physics.

5. References

[1] R.B. Spielman *et. al.*, Phys. Plasmas **5**, 2105 (1998).
[2] D.D. Ryutov *et. al,* Rev. Modern Physics, (2000).
[3] T.W. Hussey , Journal of Applied Physics, 51(**3**), 1452 (1980).
[4] S. Chandrasekhar, *Hydrodynamic and Hydromagnetic Stability* (Dover Publications Inc., New York, 1981).
[5] M. Douglas *et. al.*, Bull. of the American Phys. Soc., 42(**10**), 1878 (1997).
[6] A.C. Robinson *et. al.*, In Proceedings of the IEE International Conference on Plasma Science (1999).
[7] http://www.bicron.com/bc422Q.htm
[8] R.B. Spielman, *X-RAY DETECTOR: an X-Ray Radiation Detector Design Code*, Sandia Report, SAND85-0699.UC-37 (1990).
[9] F. Biggs and R. Lighthill, *Analytical Approximations for X-Ray Cross Sections III*, Sandia Report, SAND87-0070.UC-34 (1988).
[10] G.A. Chandler *et. al.*, Rev. Sci. Inst., 70(**1**), 561 (1999).
[11] D. Halliday and R. Resnick, *Physics* (John Wiley & Sons, New York, 1962).
[12] C. Yeh, *Handbook of Fiber Optics Theory and Applications* (Academic Press, New York, 1990).
[13] C.A. Fletcher, *Computational Techniques for Fluid Dynamics* (Springer, Berlin, 1991).

Sandia is a multiprogram laboratory operated by Sandia Corporation, a Lockheed Martin Company, for the United States Department of Energy under contract DE-AC04-94AL85000.